

MODIFICATION OF SUGARCANE BAGASSE DERIVATIVES WITH SUPERPARAMAGNETIC IRON OXIDE NANOPARTICLES, FOR THE EXTRACTION OF HYDROCARBONS

MODIFICACIÓN DE DERIVADOS DEL BAGAZO DE CAÑA DE AZÚCAR CON NANOPARTÍCULAS DE ÓXIDO DE HIERRO SUPERPARAMAGNETICAS, PARA LA EXTRACCIÓN DE HIDROCARBUROS

S. ALBUERNE-TORRES^a, O. GARCÍA-ZALDÍVAR^{d†}, A. ÁLVAREZ-DELGADO^b, A. BROWN-GÓMEZ^b, P. ARANDA^c, E. RUIZ-HITZKY^c, Y. GONZÁLEZ-ALFARO^{a†}

a) Centro de Estudios Avanzados de Cuba. Carretera San Antonio de los Baños e/ 179 y 340. Valle Grande, La Lisa, Habana, Cuba. 17100, Cuba; yorexis.gonzalez@gmail.com[†], sayli.at@cea.cu.

b) Instituto Cubano de Investigaciones de los Derivados de la Caña de Azúcar (ICIDCA), Vía Blanca 804 y Carretera Central, San Miguel del Padrón, 11000, Habana, Cuba; alvarezd@azcuba.cu.

c) Instituto de Ciencia de Materiales de Madrid, CSIC, c/ Sor Juana Inés de la Cruz 3, Cantoblanco, 28049 Madrid, España; eduardo@icmm.csic.es, pilar.aranda@csic.es.

d) Grupo de Materiales Ferroicos de Facultad de Física/Instituto de Ciencia y Tecnología de Materiales, Universidad de La Habana, San Lázaro y L, Vedado, Plaza, La Habana 10400, Cuba. osmany.garcia@gmail.com[†].

† corresponding author

Recibido 30/05/2023; Aceptado 3/10/2023

In this work, composites of magnetite nanoparticles embedded in sugarcane bagasse are obtained and characterized. The quasi-spherical shaped iron oxide nanoparticles, obtained by chemical methods, as well as the composite samples were physically characterized by different techniques. The diffraction patterns of the samples together with the EDX mapping of iron atoms on the surface of the samples confirm the homogeneous distribution of nanoparticles in these materials. The resulting composite materials retain the adsorption/absorption capacity of the bagasse as well as the superparamagnetic properties of the magnetite nanoparticles. These two combined properties facilitate the application of the nanocomposites as a hydrocarbon adsorbent material, with the potential to be easily extracted from the medium by means of an external magnetic field. The magnetic extraction of hydrocarbons broadens the versatility of the applications of the composite material described here, facilitating its dispersion in large areas of water without the need of barriers for its collection, representing a wonderful alternative for the remediation of uncontrolled oil spills.

En este trabajo se obtienen y caracterizan materiales composites formados por nanopartículas de magnetita ensambladas en bagazo de caña de azúcar. Las nanopartículas de dicho óxido de hierro obtenidas por métodos químicos presentan una forma cuasiesférica, y al igual que las muestras de los composites, fueron caracterizadas físicamente mediante diferentes técnicas físico-químicas. Los patrones de difracción junto al mapeo EDX de átomos de hierro en la superficie de las muestras, confirman la distribución uniforme de nanopartículas en estos materiales. Los materiales compuestos resultantes conservan la capacidad de adsorción/absorción del bagazo así como las propiedades superparamagnéticas de las nanopartículas de magnetita. Estas dos propiedades combinadas facilitan la aplicación del nanocomposite como material adsorbente/absorbente de hidrocarburos, con potencial para ser extraído fácilmente del medio acuoso utilizando un campo magnético externo. La extracción magnética de hidrocarburos amplía la versatilidad de las aplicaciones del material compuesto aquí descrito, facilitando su dispersión en grandes extensiones de agua sin necesidad de barreras para su recogida, representando una magnífica alternativa para la remediación de vertidos incontrolados de hidrocarburos.

PACS: Magnetic properties of nanostructures (propiedades magnéticas de las nanoestructuras), 75.75.-c; growth from solutions (crecimiento a partir de soluciones), 81.10.Dn; Other topics in magnetic properties and materials (otros tópicos en propiedades magnéticas y materiales), 75.90.+w.

I. INTRODUCTION

Sugar cane bagasse is one of the wastes generated by the sugar industry. Bagasse is the solid residual mass resulting from the process of extracting the juice from inside the stem of the cane. Also considered as an alternative energy source, bagasse is made up of insoluble granulated solids, soluble solids and a high percent of relative humidity. Depending on the humidity, the obtained densities range between 50 kg/m^3 and 96 kg/m^3 [1,2]. In general, it is reported to be composed of 40-46% insoluble granular solids, 6-8% soluble solids and 46-52% moisture [3,4]. It contains solid particles formed by two very different structures: the fibers, made up of cylindrical

(columnar) cells and hard-walled vascular tissues, and the medulla or core formed by parenchymal cells of irregular shape and thin walls of little structural strength [3,4]. The last one is found in the central region of the cane stem, it is spongy in nature and can absorb up to 20 times its own weight in water. The fibrous component, so-called pithless bagasse, can be separated using pith-removal equipment [1]. The development of depithing equipment and systems is well known in the sugar industry, which are used in the preparation of bagasse for the pulp paper industry and for manufactured of particle boards. Currently there is a trend to use dephiter

at the sugar mill with vertical rotors and different processing capacities. In Cuba two industrial models of vertical rotors depithers known SM Caribe 800 and SMCaripe 1500 were developed, and are used in the Cuban sugar industry for different purposes [5–7].

Sugarcane bagasse can be used for the absorption/adsorption of different contaminants, including hydrocarbons, due to both its chemical composition and its good adsorbent/absorbent properties [1, 3, 4, 8–11]. Currently, there is a broad variety of multifunctional composite materials in which a matrix is functionalized with nanoparticles, in which the properties of the resulting material are the combination of those of the starting components.

Magnetite iron oxide nanoparticles, with an inverse-spinel cubic structure, are widely used in obtaining composite materials due to their marked superparamagnetic behavior for particle sizes less than 20 nm. The superparamagnetic behavior is present in magnetic systems with non-interacting magnetic dipoles moments that can be easily reoriented in the direction of an applied magnetic field but return to a random configuration of the direction of their magnetic moments when the external magnetic field is removed. In other words, it is a system with no magnetic memory in which the magnetization as a function of the magnetic field can be described by a Langevin function [12].

A granulated system obtained through the anchoring and uniform distribution of these nanoparticles in a matrix, organic or inorganic, constitutes a superparamagnetic composite material called dry ferrofluid [13, 14, 16]. The property of the ferrofluid, switchable magnetizing/demagnetizing response to the external magnetic field's on/off commutation, is transferred to the porous solid by anchoring the magnetic nanoparticles in the active sites of the porous matrix [14–16].

The assembly of magnetic nanoparticles with porous solids of very diverse nature, including for instance inorganic solids as well as biopolymers and specifically lignocellulosic materials, represents an extraordinary option to develop superparamagnetic adsorbents and sorbents with a wide range of applications in environmental remediation [14, 16]. On the other hand, it is well known that diverse biomass-derived materials such as agricultural wastes have been considered as efficient and sustainable components of natural origin for the adsorption of oils and other pollutants present in contaminated water [17, 18]. The inclusion of magnetic nanoparticles such as magnetite iron oxide nanoparticles in this type of materials, including sugarcane bagasse, facilitates the recovering of the materials containing pollutants by application of external magnetic fields [14, 19–22].

A composite material, in which the superparamagnetic properties of magnetite nanoparticles are combined with adsorbent/absorbent properties of cane bagasse, improving physical-chemical interaction mechanisms, would be of great relevance for environmental remediation processes [9, 10, 13–16, 23]. The aim of this work is the obtaining of a granulated magnetite/bagasse composite and to evaluate the performance

of different components of bagasse (core and pithless bagasse) as hydrocarbons removers in polluted waters.

II. EXPERIMENTAL

The sugar cane bagasse used in this work comes from the Cuban Institute for Research on Sugar Cane Derivatives (ICIDCA). As was previously mentioned, bagasse is the solid fibrous residue that remains after the process of squeezing the stem to obtain the sugar cane juice. The obtained bagasse pith and the pithless bagasse, by-products of sugarcane processing, are shown in Fig. 1.

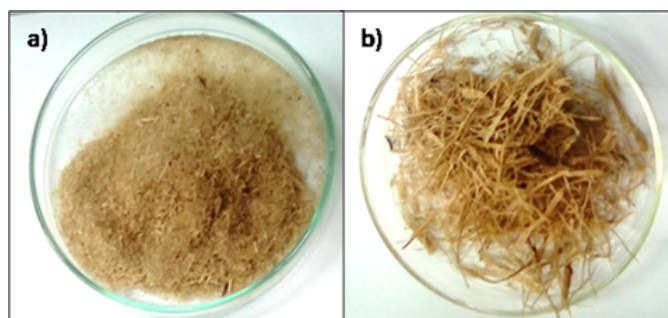


Figure 1. a) bagasse pith and b) pithless bagasse. As a size reference, the diameter of the petri dishes in the photographs are 9 cm.

After the depithing process, the by-products are sieved through different meshes. The BagM sample (pith of the bagasse) is the product that falls between the 1.19 mm and 0.15 mm meshes, while the BagD sample (pithless bagasse) corresponds to the product that remains above the 1.5mm mesh [24]. The characteristic humidity for these is 12 % and 10.69 % for BagM and BagD, respectively [24]. These two bagasse by-products, provided by Primero de Enero sugar mill, were used as organic matrix to obtain the composite.

Iron oxide nanoparticles were obtained by the coprecipitation method, according to that reported in [13, 14, 16]. High purity starting materials were used for the synthesis of iron nanoparticles. 4.86g of $\text{FeCl}_3 \cdot 6\text{H}_2\text{O}$ (Sigma-Aldrich, 99 % purity) and 3.34 g of $\text{FeSO}_4 \cdot 7\text{H}_2\text{O}$ (Sigma-Aldrich, 99 % purity) were mixed in 40 ml of ultra-pure water (18.2 M Ω cm resistivity).

The solution, placed in a silicone oil bath at 90°C, was mechanically stirred at 164 rpm until the stabilization of temperature. After that, 0.9 ml of the surfactant agent oleic acid (Sigma-Aldrich, 99 % purity) was added. The solution was kept stirring for a few seconds before adding 12 ml of dilute ammonium hydroxide up to 25 %. A reaction takes place, resulting in a black precipitate. The system is kept at 90 °C for 3 h under continuous stirring to ensure that the reaction occurs completely. Then, the precipitated solid is recovered with an iron-neodymium permanent magnet and washed multiple times with bi-distilled water until the drained water reaches a neutral pH. The resulting solid is rinsed with acetone, to remove residual surfactant, dried at room temperature in a fume hood for 24 h and grounded in a mortar. After the entire process, 1.8 g of a black powder, named magnetic

nanoparticles (NPM), is obtained. The elemental analysis, performed in a CNHS PERKIN ELMER 2400 Elemental Analyzer to estimate the weight of oleic acid respect to the total mass of the obtained material, determined the existence of an 84 % of magnetite.

To obtain the composite material, 1 g of NPM were added to 40 ml of n-heptane while the recipient is stirred in an ultrasonic bath for 15 min and then in a shaker for 5 min more to form a ferrofluid. Then, 1 g of bagasse (Bag-M or Bag-D) is added to the ferrofluid, repeating two times the former stirring procedure. The mixture is dried at room temperature in an extraction hood for 72 h and finally grounded on agate mortar. Nominally, a composite material with a 50/50 NPM to bagasse ratio was obtained. A schematic representation of whole process is represented in Fig. 2.

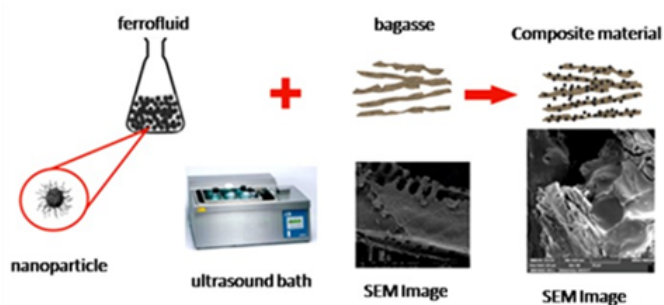


Figure 2. Protocol of preparation of the composite material.

The X-ray diffraction (XRD) characterization of the studied samples was performed in a Shimadzu, model XRD-7000, $\text{CuK}\alpha$ radiation diffractometer at room temperature. The interval 2θ scan from 10° to 80° with a step of 0.02° was set for all the samples. Additionally, a standard Si sample was measured under the same conditions to account for the instrumental contribution to the profile of the diffraction peaks.

The morphology and size distribution of the magnetic particles were determined through Transmission Electron Microscopy (TEM). Measurements were made in a JEOL JEM 2010 microscope, operating at an accelerating voltage of 120 kV. To visualize the nanoparticles, a water diluted suspension was prepared and dropped on a copper grid, superficially modified with a layer of carbon, allowing the solvent fully evaporation before performing the measurement.

The morphology of the composite material and the presence of iron in its structure were studied using field emission filament scanning electron microscopy (FE-SEM) by using a TESCAN model Mica3 OXFORD INSTRUMENTS Microscope with a coupled energy dispersive X-ray analysis system (EDS). The samples were fixed on a carbon adhesive tape on an aluminum sample holder and coated with a 10 nm film of gold to avoid charges accumulation.

The magnetic characterization was carried out in a superconducting quantum interference device (SQUID) model Quantum design MPMS XL-7T. The maximum magnetic field used was 30 kOe at room temperature. For

magnetic measurements, the granulated samples were packed in a conical bottom plastic vial and fixed to the bottom by adding a few drops of Kola Loka glue. Then, the bottom with the fixed sample was cut and attached to the sample holder of the magnetometer.

The adsorption capacity of the composites was performed by measuring the difference in mass of hydrocarbons before and after the extraction process. For that purpose, 50 ml of hydrocarbon are weighed in a 100 ml beaker and then 20 mg of the composite are added to the beaker while maintaining a constant mechanical agitation. After 1 min, following the magnetic extraction procedure reported elsewhere [13,14,16], the composite material is removed vertically by inserting a NdFeB (N50) magnet disk coated with a nickel alloy and a holding force of 17 kg. After 5 min, time needed to guarantee that the hydrocarbon not effectively adsorbed/absorbed in the composite drains back to the vessel, the beaker is then weighed and the difference in mass is calculated. The measurement was made with an analytical balance Model KERN ABT220-4M (precision grade 0.001 g). The used hydrocarbon was taken from two different areas of the Níco López refinery in Havana, with different degrees of viscosity given in API degrees by its acronym in English (American Petroleum Institute).

III. RESULTS AND DISCUSSION

The XRD pattern of the NPM/BagM composite and those of the individual components of the composite are presented in Fig. 3. The diffraction patterns of both NPM- Fe_3O_4 and the composite show the characteristic crystalline contribution, corresponding to the inverse spinel structure of the magnetite. The identification of crystallographic family of planes according to (JCPDS file No. 19-0629) is presented as well in that figure.

It is worth noting here that it is impossible differentiate magnetite (Fe_3O_4) and maghemite ($\gamma\text{-Fe}_2\text{O}_3$) from XRD patterns. However, it has been proven in previous reports [13, 16] that the coprecipitation of Fe^{2+} and Fe^{3+} salts at a controlled pH, in the presence of a surfactant, results in the precipitation of magnetite particles whose surface oxidizes to form maghemite. The superficial oxidation of magnetite to maghemite occurs through the rearrangement of the atoms without causing changes in the morphology of the nanoparticle, creating a superficial layer of maghemite on the magnetite nanoparticle [13, 16]. Therefore, magnetite nanoparticles with an outer surface layer of maghemite are most likely to be obtained.

An amorphous broadband contribution at low diffraction angles ($10^\circ < 2\theta < 40^\circ$) that correspond to the bagasse BagM it can be detected. As observed in Fig. 3, the diffraction pattern of the composite NPM/BagM presents the unaltered contributions of their individual components, which means that the functionalization procedure does not cause any changes in the starting materials. Hence, it is expected that the composite material maintains the properties of both the matrix as well as of the filler, so, the NPM/BagM would keep the adsorbent/absorbent nature of the bagasse and the

superparamagnetic behavior of magnetite nanoparticles. The diffraction pattern of the composite NPm/BagD (not shown here) presents the same behavior.

From the diffraction patterns and using the Debye-Scherrer equation, which relates the integral width of the peaks with the crystallite size, the average size of the crystallites was calculated for both isolated nanoparticles and composite systems. The instrumental contribution to the diffraction profile was considered by using a Si pattern, measured under the same conditions of those of the samples. The average crystallite size (coherent domain size) for iron nanoparticles, both in isolated nanoparticles and in composite materials, was 9.3 ± 0.7 nm, confirming that the process for obtaining the composite material does not influence the crystal growth of nanoparticles.

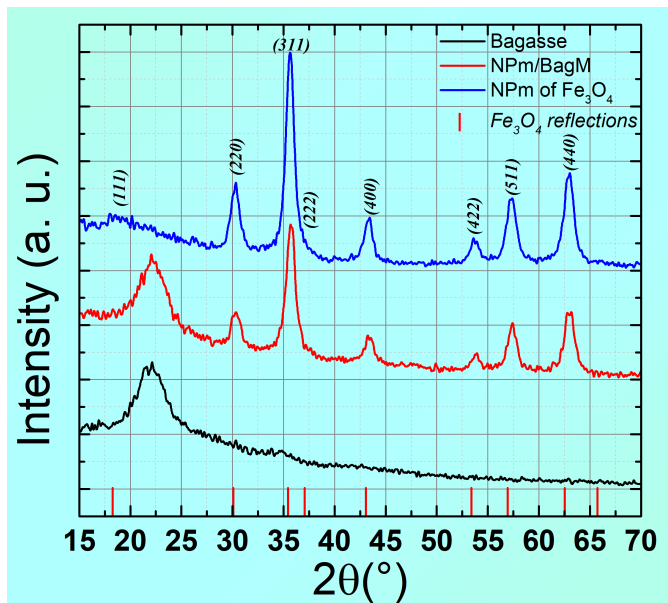


Figure 3. XRD of composite material NPm/BagM, nanoparticles of Fe_3O_4 and BagM samples.

The morphology and size of the isolated nanoparticles can be observed in the TEM image of Fig. 4. The magnetite nanoparticles (darker regions), quasi-spherical in shape, are embedded in (or coated by) oleic acid (lighter surrounding region). The particle size distribution is log-normal with an average size of 11.0 nm. This value is very close to that obtained by X-ray diffraction for the average crystallite size, suggesting the obtaining of monocrystalline nanoparticles, and is below the critical size (20 nm diameter) needed to display superparamagnetic behavior [25,26].

Fig. 5 show the SEM micrographs of both obtained composites. The Fig. 5 (top) shows the fiber structure of the pithless bagasse and the Fig. 5 (bottom) shows the high porosity structure with large cavities of the bagasse pith, as is described in the literature [27]. As it can be observed both matrices maintain their morphologies after being functionalized with the magnetite nanoparticles, so it can be expected that the composite material maintains the adsorption capacity of the

starting matrices reported in literature [27].

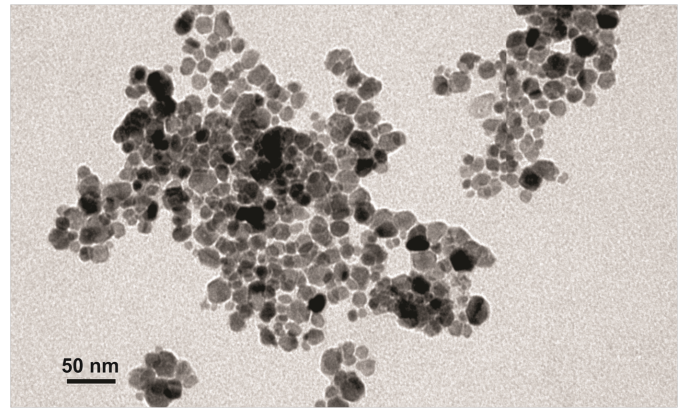


Figure 4. TEM image of isolated magnetite nanoparticles.

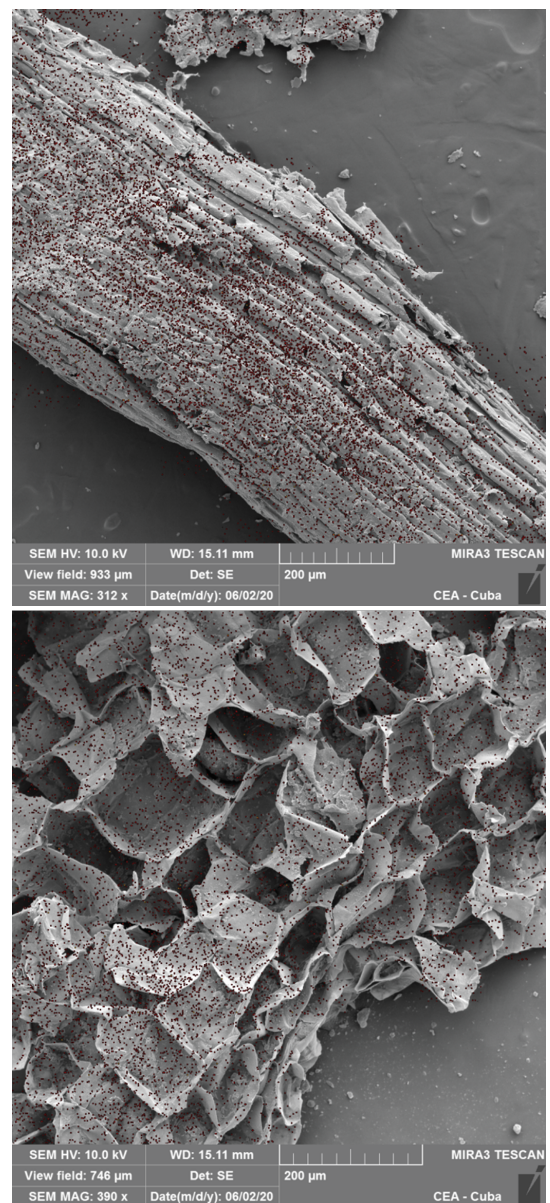


Figure 5. SEM image of the composite materials: NPm/BagD (top) and NPm/BagM (bottom).

Both images show the presence of red points that are the result of the superposition of the SEM image and the image obtained by EDX mapping of iron atoms in the same region. As can be observed, both for sample NPm/BagM and for NPm/BagD, the magnetite load is uniformly distributed throughout the entire surface of the bagasse matrix, which is fundamental for extraction.

The superparamagnetic nature of the nanoparticles and that of the composite NPm/BagM are evident from the magnetization curves in Fig. 6. They correspond to well saturated magnetic loops with near null remnant magnetization and coercive field, typical of diluted magnetic systems or systems with not-interacting dipoles moments. Similar results are obtained for NPm/BagD (not shown here).

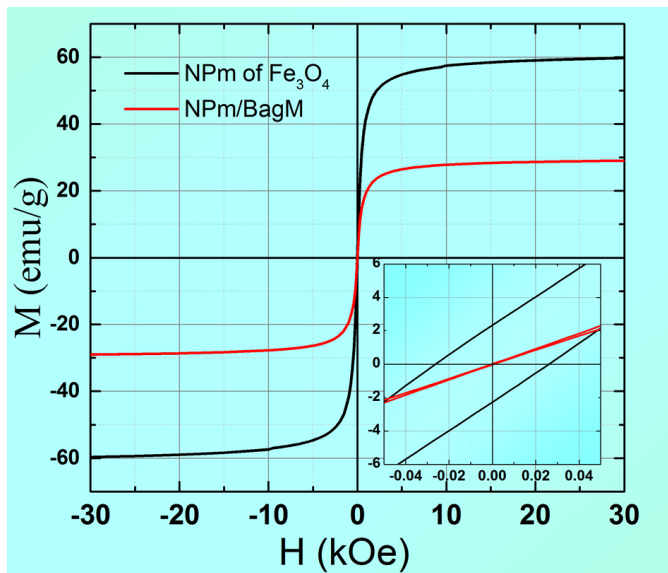


Figure 6. Magnetic hysteresis loops for the isolated nanoparticles and for NPm/BagM composite.

For massive magnetite materials, the magnetization saturation value (M_s) at room temperature is reported to be 92 emu/g [28, 29]. As it can be observed from Fig. 6, the magnetization saturation value for the isolated magnetite nanoparticles is determined to be 60 emu/g, far below of that reported for bulk systems. The difference in M_s between bulk and nanoparticles systems arise from surface effects. Below a critical size, the lack of symmetry and coordination of the outer layers of atoms at the surface of the nanoparticles effectively reduce the spin-spin coupling, leading to a decrease in magnetization [28, 29]. In a bulk material, the surface contribution is negligible, but becomes relevant with the decrease of the size as the surface to volume ratio increases.

Differences in the saturation magnetization values between the isolated nanoparticles and the composite came from the fact that the mass considered in the case of NPm/BagM is the total mass and not only that of the magnetite present in the composite.

The inset in Fig. 6 shows the region of low fields in which it can be observed, in the case of nanoparticles, a slight remnant magnetization of around 2 emu/g and a coercive

field of around 20 Oe. This result suggests the existence of agglomerates, possibly of the largest particles, in which a weak magnetic interaction between their dipole moments is established. In contrast, no remnant magnetization or coercive field can be observed for the NPm/BagM, probably due to the fact that the uniform distribution of the magnetite load in the composite avoids the nanoparticles agglomeration.

It is expected that the obtained composite materials maintain the properties of the matrix and the filler. If these properties are maintained within a certain range, the final composite material would maintain the adsorbent/absorbent nature of the bagasse matrix and the superparamagnetic behavior of the nanoparticles.

Table 1. Absorption capacity of composites

RAW ρ (g/cm ³)	Absorption NPm/BagM (g _{Hyd} /g _{BagM-NPm})	Absorption NPm/BagD (g _{Hyd} /g _{BagD-NPm})
light (<870 kg/m ³) 64.65 API	8.55	6.52
	8.72	6.48
	8.63	6.51
Medium (<870-920 kg/m ³) 25.41 API	7.03	4.93
	7.00	4.90
	7.02	4.89

In order to determine the absorption capacity, expressed in grams of hydrocarbon per grams of used composite material, a study was carried out following the procedure described in the experimental section. The results, presented in Table 1, compare the values of the hydrocarbon absorption measured for two crude fuels with different density values in the two studied adsorbent/absorbent matrices. Three different experiments were run for each crude fuel with no significant statistical differences.

The absorption capacity values for the bagasse pith composite NPm/BagM are relatively higher than those obtained for the pithless bagasse composite NPm/BagD. These results are directly related to the microstructural characteristics of the organic matrix. As it was described previously, the bagasse pith presents a highly porous structure with large cavities. This microstructure, similar to foam, has a larger surface area density than that of pithless bagasse, facilitating the functionalization of nanoparticles at its surface and so improving the magnetic separation process. At the same time, the microstructure has a larger exchange area and cavities that improve the adsorption and absorption of hydrocarbons. In fact, both composites have higher values of absorption capacity than those reported in literature for bagasse (4.39 g_{Hyd}/g_{Bag}) [30], being the magnetic extraction easier to perform than that of the reported method. In addition, the material resulting from the extraction of the crude has a higher heat capacity than the original bagasse because it contains residual oil and can therefore be advantageously reused as fuel [2, 30].

Furthermore from Table 1 it can be deduced a decrease in the absorption with the increase in hydrocarbon density. It was previously reported [29] that the decrement in absorption capacity with density is related to the viscosity of the fluid; the

lower the viscosity of the hydrocarbon, the better it will flow inside the material, completely filling its pores and cavities.

IV. CONCLUSIONS

The successful preparation of a composite material by the assembly of bagasse and magnetic iron oxide nanoparticles has been reported. A detailed characterization of the physical properties of these nanoparticles allows controlling the nature of the resulting composites. The diffraction patterns of such nanoparticles are mainly consistent with the presence of magnetite phase. The formation of maghemite, although in small quantities as a thin outer layer of the nanoparticle cannot be ruled out. The combined results of TEM and DRX confirm the formation of quasi-spherical monocrystalline nanoparticles. These results are consistent with the slim hysteric loop obtained for nanoparticles corresponding to both composites.

The composite materials preserve the superparamagnetic behavior and the adsorption/absorption capacity of the pristine magnetite nanoparticles. The absorption capacity tests confirm that the extraction mechanism using these materials is more effective than others previously reported and reveal that bagasse pith has higher absorption capacity than pithless bagasse. The application of bagasse as a hydrocarbon collector material in aqueous medium, with the potential to be extracted from the medium by means of an external magnetic field increases the performance of the material, enabling its dispersion in large areas of water without the need of barriers for its collection. Therefore, these sustainable materials that allow the use of lignocellulosic agro-food waste are an attractive alternative to eliminate hydrocarbons in water and especially in catastrophes caused by oil spills.

ACKNOWLEDGEMENTS

This work was supported by the grant PN211LH008-006 from the Cuban National Nanoscience and Nanotechnology Program (PN3). P.A. and E.R.-H. acknowledge financial support by the MCIN/AEI/10.13039/501100011033 (Spain, project PID2019-105479RB-I00), as well as LignoCOST (E.U. COST Action CA17128).

REFERENCES

- [1] G. A. Roca Alarcón, C. Glauco Sanchez, E. Olivares Gómez, L. A. Barbosa Cortez, *Caracterización del bagazo de la caña de azúcar. Parte 1: características físicas* (Centro de Estudios de Eficiencia Energética-CEEFE, Universidad de Oriente, Santiago de Cuba, Cuba, 2006).
- [2] A. D. Rodríguez Arias y L. B. Rosabal Ponce, *Anales de la Academia de Ciencias de Cuba* **7**, 78 (2017).
- [3] L. González, *ICIDCA sobre los Derivados de la Caña de Azúcar* **17**, 4 (1983).
- [4] J. L. Correa, *Revista ICIDCA. Editorial Científico-Técnica*, 77 (1982).
- [5] *Handbook of sugar cane Derivatives* (Third Edition, MINAZ. 2000).
- [6] O. Triana, M. Leonard, F. Saavedra, N. Fernández, y G. Gálvez, *Atlas del Bagazo de la Caña de Azúcar*, Mexico City (México) GEPLACEA 1990, Grupo de Países Latinoamericanos y del Caribe Exportadores de Azúcar. https://digitalcollections.qut.edu.au/1529/1/Atlas_of_Sugarcane_Bagasse.pdf.
- [7] O. Almazán del Olmo, A. Hernández Gutiérrez, M. A. Brizuela Herrada, O. Carvajal Cabo, G. N. Arias Polo, y N. Fernández Rodríguez, *El bagazo de la caña de azúcar, conocimiento y potencial* (La Habana, Editorial ICIDCA, 2013).
- [8] A. Armada, E. Barquinero, y E. Capote., *ICIDCA sobre los Derivados de la Caña de Azúcar XLII*, 96 (2008).
- [9] V. Raj, M. Singh Chauhan, and S. Lal Pal, *Chemosphere* **307**, 135825 (2022).
- [10] Aruna, N. Bagothia, A. Kumar Sharma, and S. Kumar, *Chemosphere* **268**, 129309 (2021).
- [11] G. Lemessa, N. Gabbiye, and E. Alemayehu, *Water Practice and Technol.* **18**, 393 (2023).
- [12] Y. Fernández-Afonso, A. Maury-Toledo, O. García-Zaldívar, M. A. Hernández-Landaverde, R. Ramírez-Bon, J. M. Yañez-Limón, S. Díaz-Castañón, Y. González-Alfaro, y F. Calderón-Piñar, *Rev. Cubana Fis.* **34**, 3 (2017).
- [13] Y. González- Alfaro, *Ensamblado de nanopartículas magnéticas de magnetita a sólidos porosos por interacción con ferrofluidos para el desarrollo de materiales multifuncionales*, PhD Thesis, Universidad Autónoma de Madrid, Madrid, 2016.
- [14] E. Ruiz-Hitzky, P. Aranda, and Y. González-Alfaro. Spanish Patent 201030333, 2010; PCT ES2011/070145, (2011).
- [15] M. F. Horst, V. Lassalle, and M. L. Ferreira, *Front. Environ. Sci. Eng.* **9**, 746 (2015).
- [16] Y. González-Alfaro, P. Aranda, F. M. Fernandes, B. Wicklein, M. Darder, and E. Ruiz-Hitzky, *Adv. Mater.* **23**, 5224 (2011).
- [17] A. Bhatnagar, M. Sillanpaa, and A. Witek-Krowiak, *Chem. Eng. J.* **270**, 244 (2015).
- [18] A. Sanguanwong, A. E. Flood, M. Ogawa, R. Martin-Sampedro, M. Darder, B. Wicklein, P. Aranda, and E. Ruiz-Hitzky, *Journal of Hazard. Mat.* **417**, 126068 (2021).
- [19] Ph. Zito and H. J. Shipley, *RSC Adv.* **5**, 29885 (2015).
- [20] K. B. Debs, D. S. Cardona, H. D. T. da Silva, N. N. Nassar, E. N.V.M. Carrilho, P. S. Haddad, and G. Labuto, *J. Environ. Mgt.* **230**, 405 (2019).
- [21] D. S. Cardona, K. B. Debs, S. G. Lemos, G. Vitale, N. N. Nassar, E. N. V. M. Carrilho, D. Semensattoe, and G. Labuto, *J. Environ. Mgt.* **242**, 362 (2019).
- [22] G. da Costa Cunha, N. C. Pinho, I. A. Alves Silva, L. Santos Silva, J. A. Santana Costa, C. M.P. da Silva, and L. P.C. Romão, *J. Environ. Mgt.* **247**, 9 (2019).
- [23] R. Juwita, C. Irawan, R. Jelita, and I. F. Nata, *IOP Conf. Ser.: Mater. Sci. Eng.* **980**, 012006 (2020).
- [24] O. Carvajal, J. Puig, J. A. Leal, y M. E. Rodríguez, *ICIDCA sobre los Derivados de la Caña de Azúcar* **19**, 19 (1985).

- [25] C. T. Yavuz, J. T. Mayo, W. W. Yu et al., *Science* **314**, 964 (2006).
- [26] L. Martín, M. Knobel, and J. Marcelo, *Rev. Cubana Fis.* **20**, 9 (2003).
- [27] D. Dopico-Ramírez, V. León-Fernández, C. Díaz-López, E. Peña-Sartorio, y M. Isabel Céspedes-Sánchez, *ICIDCA Sobre los Derivados de la Caña de Azúcar* **50**, 29 (2016).
- [28] R. M. Cornell and U. Schwertmann. *The Iron Oxides: Structure, Properties, Reactions, Occurrences and Uses. 2nd Ed.* (Wiley VCH Weinheim, Germany. 2004)
- [29] A. Gómez, Preparación de nanopartículas magnéticas uniformes y de alta cristalinidad, PhD Thesis, Universidad Complutense de Madrid, Madrid, (2009).
- [30] A. Brown-Gómez, J. Alberto Pérez-Hernández, y Y. Izquierdo-González, *ICIDCA sobre los derivados de la caña de azúcar* **49**, 10 (2015).

This work is licensed under the Creative Commons Attribution-NonCommercial 4.0 International (CC BY-NC 4.0, <http://creativecommons.org/licenses/by-nc/4.0>) license.

